

CURVED-EDGE DISPLACEMENT SENSOR FOR SPINDLE DYNAMIC IDENTIFICATION

Seungjoo Lee¹, Jungsub Kim¹, ChaBum Lee¹, and Gregory W. Vogl²

¹J. Mike Walker '66 Department of Mechanical Engineering
Texas A&M University
College Station, TX, USA

²National Institute of Standards and Technology (NIST)
Gaithersburg, MD, USA

INTRODUCTION

A spindle plays the most important role on machine tools since it heavily influences the productivity and efficiency of the machine [1]. Therefore, the technological demands on spindles toward greater accuracy and efficiency have been significantly highlighted in recent years. Along with the development of spindle technologies, the significance of monitoring, diagnosing, and predicting spindle conditions including its dynamic behavior has also been emphasized. Identification of the spindle dynamics such as stiffness and damping effects may provide useful information of tool life, tool integrity, and quality of the produced part features, including shape and surface roughness [1]. Furthermore, monitoring the spindle's dynamic condition can prevent unexpected failures and reduce the downtime of machines.

Conventionally, capacitive sensors (CS) are used for the identification of spindle dynamics due to the sensors' high bandwidth and lack of sensitivity with respect to target material [2]. Multiple sensors are mounted on the rotating shaft in the X-, Y-, and Z-axis direction to measure the conditions of the spindle. The CS, however, are calibrated with flat surfaces, which may cause measurement error while obtaining data with cylindrical targets because different responses result from a flat surface versus a curved surface [3]. Possible measurement errors may include noise and a nonlinearity of displacement due to the curved target surface when monitoring the spindle condition using CS.

Spindle dynamic identification technologies, other than CS, have been widely studied. Slatter et al. investigated monitoring the spindle condition using giant magneto-resistive sensors and found out that the sensor system is capable

of measuring displacements with a resolution of better than 0.5 μm with high repeatability [4]. Postel et al. studied a method to estimate the cutting forces and vibrations of the milling tool using accelerometers and discovered that the cutting force and displacement estimations were within 80% of the measured values [5]. Lee et al. proposed a novel sensing methodology for a curved surface using lasers based on curved-edge diffraction [3]. Lee et al. compared the results of their new method with conventional CS and observed a 0.017% discrepancy over the full measurement range.

In this study, a curved-edge sensor (CES) based on curved-edge diffraction was developed to identify system behavior. The CES was compared with CS via run-out measurements and impact tests. In addition, the CES will be compared with a three-axis force sensor to monitor the force applied while cutting a part.

CURVED-EDGE SENSOR

In this study, the CES is used to measure displacements of a curved shaft. Due to the limitations of understanding curved-edge diffraction, it is difficult to define an illumination of the edge by different wavefronts, so the CES was investigated through experimentation. Figure 1 shows the schematics of the CES measurement system, which consists of four avalanche photodetectors (APDs), prisms, and two laser diodes (LDs). The laser light is first incident on the curved surface of the spindle shaft with a radius R , and then the interaction of the transmitted waves, reflected waves, edge-diffracted waves, and edge-excited waves are detected by four APDs. Signals related to displacements along the X-axis and Y-axis are measured by APDs 3 & 4 and APDs 1 & 2, respectively. The diffracted and transmitted

components interact to form fringes, and the intensity of the fringe pattern is sensed by the APD. The APD output changes with the position of the curved edge, which can be converted into the displacement of the curved edge.

The output laser beam power of the two laser diodes is nominally 870 μW , and the diodes were oriented as a result of the polarizations of the beams to yield similar incident powers for the APDs. The incident powers for the X-axis APDs were 210 μW and 200 μW , and the incident powers for the Y-axis APDs were 150 μW and 155 μW . A low-pass filter of 15 KHz was applied to all APD signals to reduce the high frequency electric noise of the APD output.

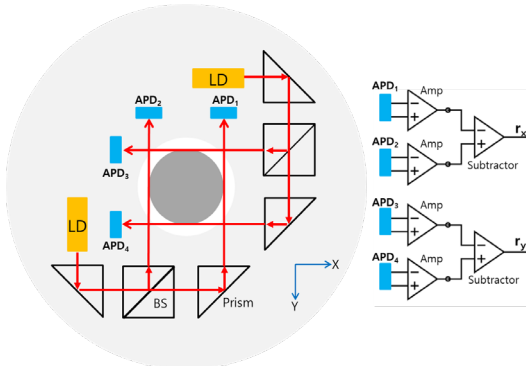


FIGURE 1. Schematics of CES measurement system and amplifier.

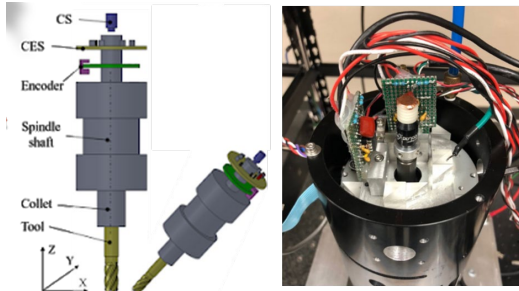


FIGURE 2. Schematic and picture of spindle system with CES.

The sensor output of the X- and Y-axes are expressed as

$$V_{out,x} = k_3 V_3 - k_4 V_4 \quad (1)$$

$$V_{out,y} = k_1 V_1 - k_2 V_2 \quad (2)$$

where $V_{out,x}$ and $V_{out,y}$ are the calibrated measurement of the CES for the X- and Y-axis, respectively, the k_i variables are gain factors, and the V_i variables are the filtered APDs signals. The APDs used in this experiment have

a sensing diameter of 500 μm . The CES was designed to measure the spindle shaft diameter of 12.7 mm. The developed sensor was then mounted inside the spindle as shown in Figure 2.

CALIBRATION

A calibration test was carried out using the CS and CESs, simultaneously, but first, the CSs were calibrated for use with a curved surface. A separate capacitive sensor was calibrated by the manufacturer with a flat target. This capacitive sensor measured a flat target fixtured on the stage of a linear positioning system, while a different CS measured a curved target (a 12.7 mm diameter rod) fixtured on the stage. By comparison, each capacitive sensor was calibrated within the range of 500 μm for measurement of a 12.7 mm diameter rod, which has the same nominal diameter as the shaft of the experimental spindle system. The sensitivities of the CS were 13.8 $\text{mV}/\mu\text{m}$ and 10.7 $\text{mV}/\mu\text{m}$ for the X- and Y-axis, respectively.

The calibrated CS were then used to calibrate the sensitivities of the CESs. A 12.7 mm diameter rod was mounted on a manual XY stage and installed at the center of the CESs to calibrate the CES system outputs. Two CS were also aligned along the X- and Y-axis of the CES system. Then, the rod was moved manually in either the X- or Y-axis direction and the CES and CS signals were measured with a sampling frequency of 10 kHz. Figure 3 shows the measured data, with the abscissa values (displacements) from the calibrated CS outputs and the ordinate values (voltage outputs) from the CES system. The CES sensitivity along the X- and Y-axis directions were 0.502 $\text{V}/\mu\text{m}$ and 0.503 $\text{V}/\mu\text{m}$, respectively, with a standard deviation of 1.0% and 1.2%, respectively, within the output range of $\pm 10\text{V}$.

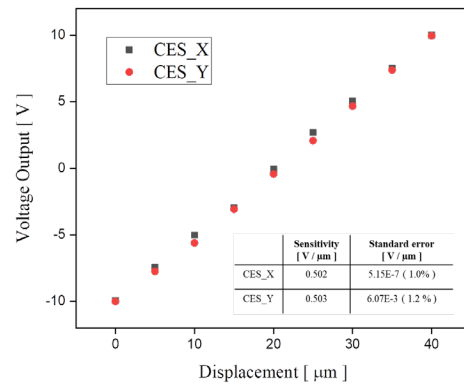


FIGURE 3. CES calibration of X- and Y-axis.

The CES resolution along the X- and Y-axis was also estimated. While the air-bearing spindle was stationary, the CES data were collected for 10 seconds, as seen in Figure 4. The CES resolution was estimated to be approximately 20 nm peak-to-peak.

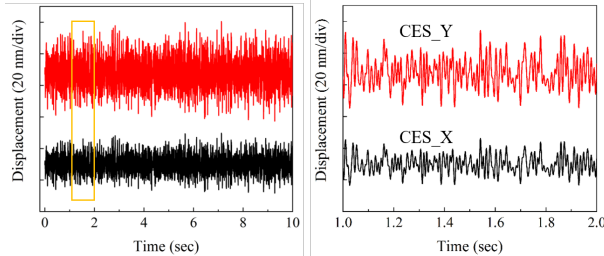


Figure 4. CES resolution test results. The subfigure to the right shows the data contained in the yellow rectangle seen in the subfigure to the left.

STIFFNESS TEST

The stiffness represents a ratio of force and displacement. The calibrated CESs were used to measure the radial stiffnesses of the air-bearing spindle, and a capacitive sensor was used to measure the axial stiffness (see Figure 2). Figure 5 shows the CES and CS displacements versus applied force. The force was applied at the tool tip to identify the displacement change with the force. The 3 x 3 stiffness (N/μm) matrix of the spindle was achieved as:

$$\begin{bmatrix} k_{xx} & k_{xy} & k_{xz} \\ k_{yx} & k_{yy} & k_{yz} \\ k_{zx} & k_{zy} & k_{zz} \end{bmatrix} = \begin{bmatrix} 4.695 & 0.264 & 0 \\ 0.242 & 4.762 & 0 \\ 0 & 0 & 12.048 \end{bmatrix} \text{ N}/\mu\text{m} \quad (3)$$

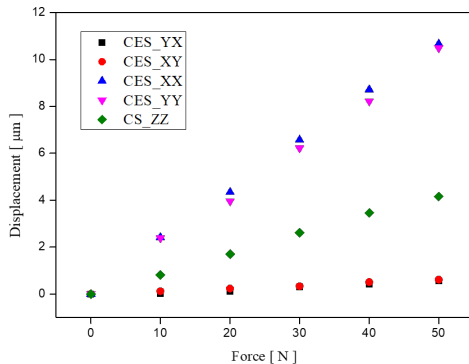


FIGURE 5. Displacement results of the CS and the CES systems according to the force applied.

IMPACT TEST

The dynamic characteristics of the spindle were also determined using CS and CES

measurement systems. The magnitude and phase plots of the spindle system with two different sensors are shown in Figure 6. The experiments were carried out using an impact hammer with an Agilent 35670A Dynamic Signal Analyzer. The CES and CS systems were implemented at the same position of the shaft. The first peak obtained by the CES and CS outputs appears at different values of about 42 Hz, showing satisfactory agreement.

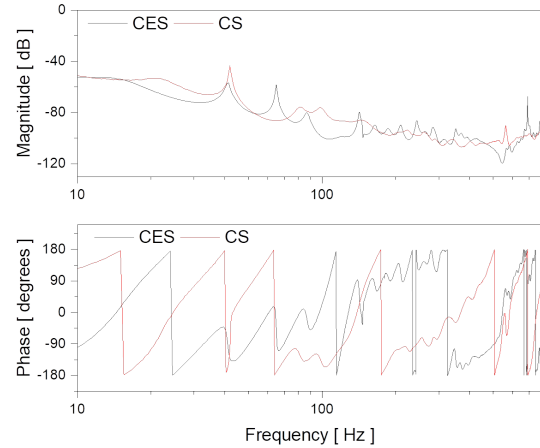


Figure 6. Impact test comparison between CS and CES outputs.

ROTATION TESTS

Data were collected at different speeds ranging from 500 rpm to 3500 rpm to measure the run-out of the cylindrical surface of the shaft at the same shaft position. The radial run-out measurements using the CS and CES systems were compared at identical X- and Y-axis positions. Data were obtained using a National Instruments LabVIEW data acquisition board.

Figure 7 shows the comparison of CS and CES outputs at spindle speeds of 1200 rpm and 2520 rpm. The overall tendency of the run-out measurements for both speeds showed similar results with a slight difference in the measurement values due to different characteristics of each CES and the CS. At 1200 rpm, the CES and CS outputs had variations of approximately 4 μm. The differences in the measurement values may be caused by the different responses of the CS with flat and curved surfaces. For the CES, on the other hand, lasers were positioned incident to the curved surface of the shaft that detect the displacement of the surface regardless of the shape of the target surface; the CES values are

mainly dependent on the calibration results based on curved-edge diffraction. For other rotation speeds, the outputs of the curved-edge sensors and capacitive sensors agreed well with respect to displacements and the run-out shape.

At the speed of 2520 rpm at which the spindle rotated at its first natural frequency (42 Hz), as seen in Figure 7, the CES and CS systems showed a similar tendency that the Lissajous pattern showed an oval shape with the displacement of approximately 6 μm in the X-axis direction and 4 μm in Y-axis direction.

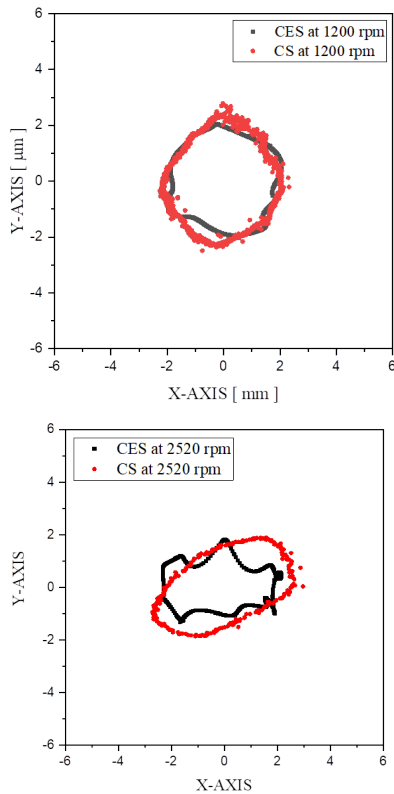


Figure 7. Run-out measurement comparison using CS and CES systems at 1200 rpm (top) and 2520 rpm (bottom).

FUTURE WORK – CUTTING EXPERIMENT

To test the CES system for estimating cutting forces, a cutting experiment was conducted and the estimated force vector (= stiffness matrix \times CES output vector) could be compared with the three-axis force sensor results.

Figure 8 shows a picture of the cutting experiment. The force changes, measured from the force sensor mounted underneath the workpiece, will be compared with the forces estimated from the CES displacements,

measured simultaneously during the cutting process. For future work, parts will be machined under various cutting conditions, and then the results obtained by the CES system and the three-axis force sensor will be compared in terms of resolution, dynamic characteristics, noise, etc. to see if the CES can be used for robust cutting force measurements.

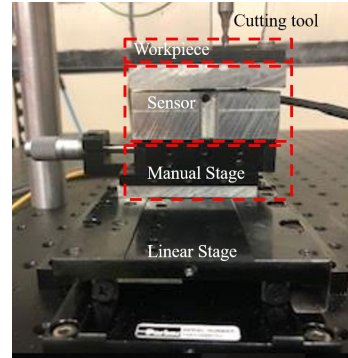


FIGURE 8. Picture of the cutting experiment.

CONCLUSION

In the study, a CES system was developed to observe the static and dynamic spindle behavior. The dynamic characteristics of the CESs were compared with conventional sensors to verify the high potential of the CES as an alternative spindle monitoring sensor due to its cost-effective capability of identifying spindle dynamics. The results of the experiments are as follows:

- 1) The X- and Y-axis sensitivities of each CES were found to be 0.502 V/ μm and 0.503 V/ μm with a standard deviation of 1.2% and 1.0%, respectively, in the 40 μm range.
- 2) Using the CES, the dynamic system characteristics were determined. It was found from the run-out measurements and impact testing that the dynamic system behaviors measured from the curved-edge sensors showed fair agreement with those from the conventional sensors.

DISCLAIMER

Certain commercial equipment, instruments, or materials are identified in this paper in order to specify the experimental procedure adequately. Such identification is not intended to imply recommendation or endorsement by the National Institute of Standards and Technology, nor is it intended to imply that the materials or equipment identified are necessarily the best

available for the purpose.

ACKNOWLEDGEMENT

This research has been supported by DOC-NIST grant (7352023-00) entitled “On-machine sensing technology for achieving high precision, high productivity, and low power in robotic manufacturing”.

REFERENCES

- [1] Kim, J., Zhao, S., Kim, G. H., & Lee, S. K. (2013). Rolling bearing-suspended spindle run-out control using repetitive control and adaptive feedforward cancellation. *International journal of Precision engineering and Manufacturing*, 14(12), 2171-2178
- [2] Marsh, E. R. (2010). *Precision spindle metrology*. DEStech Publications, Inc.
- [3] Lee, C., Mahajan, S. M., Zhao, R., & Jeon, S. (2016). A curved edge diffraction-utilized displacement sensor for spindle metrology. *Review of Scientific Instruments*, 87(7), 075113.
- [4] Slatter, R., Holland, L., & Abele, E. (2016). Magneto-resistive sensors for the condition monitoring of high-frequency spindles. *Procedia CIRP*, 46(1), 177-180.
- [5] Postel, M., Aslan, D., Wegener, K., & Altintas, Y. (2019). Monitoring of vibrations and cutting forces with spindle mounted vibration sensors. *CIRP Annals*, 68(1), 413-416.